

Analysis of 6-pole IPM synchronous motor with tangential magnets using finite element method

Abstract. The paper deals with the analysis of the 6 pole interior permanent magnet (IPM) synchronous motor with tangential magnets. To determine the magnetic field distribution in the considered motor the finite element method (FEM) has been applied. Simulations were performed for different positions of the magnets on the chords of the rotor package. The goal of performed studies was minimization of the magnetic flux leakage (understood as the flux between poles not crossing the air-gap) with respect to the high values of the analyzed functional parameters of the considered motor.

Streszczenie. W artykule przedstawiono wyniki analizy sześciobiegunowego silnika synchronicznego o magnesach umieszczonych cięciwowo w pakiecie wirnika. Do wyznaczenia rozkładu pola magnetycznego wykorzystano metodę elementów skończonych. Wykonano obliczenia symulacyjne zmieniając położenie magnesów na cięciwach pakietu wirnika. Na podstawie analizy rozkładów pola magnetycznego i wyznaczonych parametrów funkcjonalnych wytypowano strukturę najlepiej ograniczającą skutki bocznikowania magnesów. (Polowa analiza sześciobiegunowego silnika synchronicznego z magnesami umiejscowionymi cięciwowo).

Keywords: synchronous motor with tangential magnets, finite element method, magnetic bridge.

Słowa kluczowe: silnik synchroniczny z magnesami cięciwowymi, metoda elementów skończonych, mostek magnetyczny.

Introduction

Global trends in energy savings as well as development of the power electronics and manufacturing technology of the permanent magnets have led to dissemination of a permanent magnet synchronous motors (PMSM). By application of high energy density product $(BH)_{max}$ rare earth magnets the PMSM offers the highest power density among others types of the electrical machines. Moreover, to reduce costs, it is possible to use the stator sheets of mass produced asynchronous motors in the design process of the PMSM [2]. Of course, when using ready made stator sheets the changes in the design and manufacturing of rotor subcomponents are needed. For example, to reduce the cost of the rotor production and increase utilization of ferromagnetic materials the investigations related to application of soft magnetic composites (SMC) are being conducted [12, 13]. The advantage of SMC technology is possibility to manufacture the rotor core in almost single process technology without wasted material.

In general in the PMSM with radial direction of the magnetic flux in the air-gap of the machines the two major topologies of magnet placement can be distinguished: a) surface permanent magnet (SPM) machines with magnets mounted on the surface of the rotor core and b) interior permanent magnet machines (IPM) with magnets buried into the rotor core [8]. In the SPM motors the magnets are exhibited to the alternating magnetic field caused by slotting of the machine and non-sinusoidal space distribution of the magnetomotive force (mmf) excited by the winding. As a result the eddy current losses appear in the magnets. Therefore methods for reducing these losses are under intensive development. In [9, 10] authors proposed an interesting design with segmented magnets in order to reduce level of eddy current losses in the permanent magnets. From the other hand in order to achieve highest value of effective flux of PM the structures of the rotors that minimize the flux leakage are searched for. In the IPM synchronous machines the minimization of flux leakage is achieved by proper design of magnetic barriers between poles that allows for improvement of the functional parameters of the machine [1, 3].

For optimization of known and development of the new structures of the PMSM the precise models of the electromagnetic phenomena in such machines are needed. Initially for the electromagnetic calculations of the PMSM machines the equivalent circuit models basing on the lumped parameters have been employed. In the circuit

models taking into account the eddy currents effects and presence of highly saturated areas of ferromagnetic cores (especially visible for the IPM machines) is a difficult task. The level of saturation and eddy current losses have impact, among other, on the operating point and efficiency of the machine. Therefore the accuracy of such models soon became insufficient for need of the designers and researchers dealing with the PMSM. In consequence in spite of the circuit models the field models using finite element method (FEM) have become commonly used. Initially FEM models have been used to determine the parameters of the equivalent circuit [4, 5, 11].

In this paper, the authors focused on the analysis of influence of the radial placement of the tangential magnets on the functional parameters of 6-pole IPM synchronous motor. The simulations have been performed using the FEM model of the PMSM elaborated in the professional FEM package Maxwell. Discussed in the paper case study problem is a part of research activities conducted in realization of the project No. POIG.01.01.02-00-113/09 – "New generation of electric drives for the mine pumps and fans" co-financed by the European Union through the European Regional Development [2, 6, 7].

FE model of the IPM synchronous motor with tangential magnets

The field model of 6-pole IPM synchronous motor with tangential magnets has been elaborated in the professional FEM package - Maxwell. Due to the symmetry of the magnetic circuit of the studied motor (Fig. 2) the model was developed for the one pole pitch of the machine.

The studied design of the motor has been based on the stator of 6 pole asynchronous motor with mechanical size 100. The properties of the electric sheet utilized for the stator have been determined during the no load test of the base asynchronous motor. The eddy current K_e , hysteresis K_h and excess core loss K_c coefficients have been determined and introduced to the material model implemented in Maxwell environment for calculating the core losses using following formula

$$(1) \quad \Delta P_{Fe} = K_h f (B_m)^2 + K_e (f B_m)^{1.5} + K_c (f B_m)^2$$

where B_m is the amplitude of the AC flux component, f is the frequency, K_h is the hysteresis core loss coefficient, K_c is the eddy-current core loss coefficient, and K_e is the excess core loss coefficient.

The model has been suited to determine: the magnetic field distribution, the distribution of the radial component of the magnetic flux density in the air-gap of the machine, the cogging torque characteristic, back *emf* waveforms at no load state, the torque vs. stator current i_{ph} and the load angle α characteristics as well as the torque ripple factor, total harmonic distortion factor of the back *emf* waveforms and space distribution of the radial component of magnetic flux density in the air-gap of the machine.

The major dimensions of the magnetic circuit, sizes and arrangement of permanent magnets and the shape of the magnetic areas between poles (magnetic barriers) have been parameterized in order to enable optimization of the rotor structure.

Results

A number of simulations have been performed using elaborated model. The motors with different shapes of the magnetic barriers have been studied. The task was to assess the impact of the shape of magnetic bridges on discussed parameters of the motor. Two design variables have been imposed: radial placement of the magnet and width of the ferromagnetic bridge between magnets. The systematic review of the design space have been performed starting from the rotor construction with the thinnest magnetic bridge, i.e. when magnets are placed close to the air-gap - M1 (Fig. 1a) through the structure with the longest magnetic barrier, marked as M2 (Fig. 1b) to the rotor with the thickest magnetic bridge, i.e. when magnets are placed relatively close to the shaft - M3 (Fig. 1c).

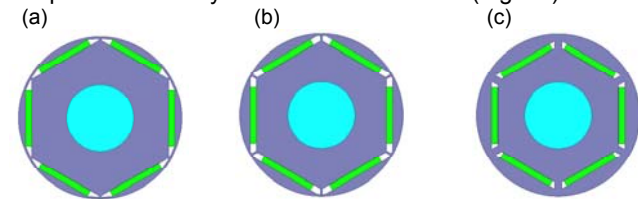


Fig. 1. Structures of considered rotors: a) M1; b) M2; c) M3

In order to enable comparative analysis the permanent magnet size as well as the air-gap length, and stator shape have been kept unchanged for studied variants. Also the winding layout and number of turns in the stator slots have been the same over investigated rotor constructions. Studied geometries have been discretized using triangular elements; the mesh density has been similar for all studied cases and equal to about 20 000.

Determined magnetic field distributions for discussed variants at on no load state (i.e. when currents in windings are equal to 0 A) have been shown in Figs. 2 to 4. Analyzing the distributions it can be noted that highest saturation level occurs in the motor with rotor denoted as M1 while in motors with rotors M2 and M3 the level of saturation is lower. The saturation of the magnetic bridges is related to the value of the flux leakage, intuitively the highest value of this flux should have the motor with the rotor construction denoted as M3. As a result the lowest exploitation of the magnetic flux of permanent magnet for producing the electromagnetic torque can be expected.

On the low exploitation of the magnetic flux of the magnets indicates also the value of the radial component of the magnetic flux density in the air-gap - see Fig. 3. The rated load has been defined for the *RMS* value of the phase current i_{ph} equal to 6A and torque angle α between rotor and stator field axes equal to 70°. Focusing on the distributions it can be seen that the highest value of the amplitude of the radial component of the magnetic flux density B_r is obtained for the structure M1, i.e. when the magnet is placed closest to the air-gap of the machine.

However, when studying the impact of stator slotting it can be noted that the smoothest distribution of B_r is obtained for the rotor M3.

For the quantitative assessment of the obtained distributions the Fourier analysis has been employed. The summary report for the distributions of B_r at rated load conditions has been given in Table 1. It confirms that the *RMS* and first harmonic values are the highest in M1. However looking at the total harmonic distortion factor (THD_B) of the obtained space distribution of the B_r it can be noted that due to stator slotting and constant length of the air-gap the impact of magnetic bridge shape is minor.

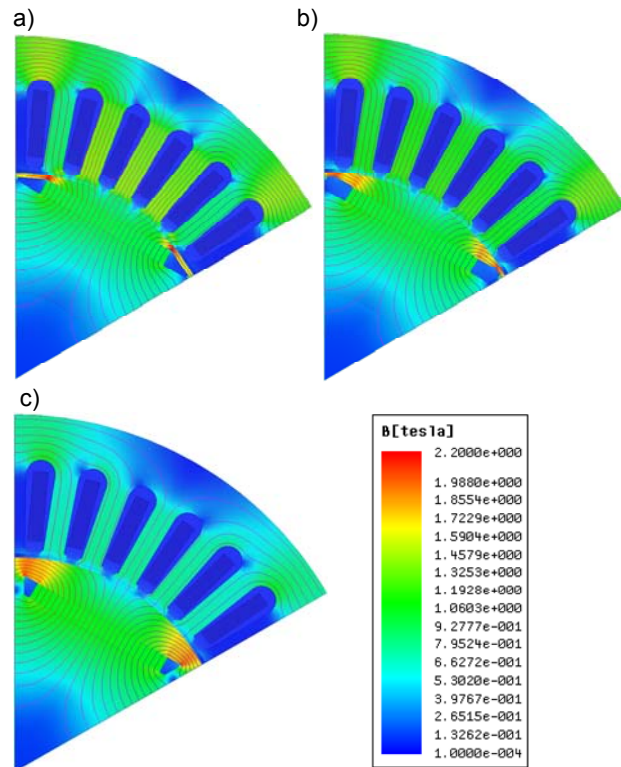


Fig. 2. Distribution of the magnetic flux density and the flux lines for the motors with rotors denoted as a) M1; b) M2 and c) M3 for no load state i.e. when phase *RMS* value of the supply current is equal to 0, $i_{ph}=0A$

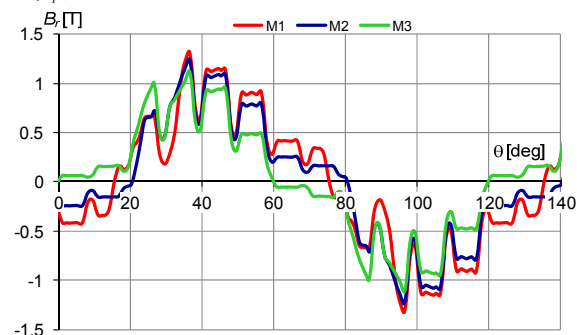


Fig. 3. Distribution of the radial component of the magnetic flux density in the air-gap of the machine at full load state ($i_{ph}=6A$ and $\alpha=70^\circ$)

In the next step the analyses of the induced at no current state electromotive force (*emf*) have been performed. The determined waveforms of phase back *emf* (E) for discussed rotor structures have been shown in Fig. 4. On the basis of presented results it can be seen that the highest value of the *RMS* as well as of the first harmonic has the motor with the rotor denoted as M1. The decrease of the back *emf* value when increasing the distance between permanent magnet and the air-gap of the machine can be

observed. Nevertheless the presence of slot harmonics is highly visible when magnets getting closer to the air-gap.

Table 1 Summary report of the radial component of the magnetic flux density in the air-gap for rated load conditions ($i_{ph} = 6A$, $\alpha = 70^\circ$)

Rotor structure	B_{r1}	THD_B	B_{RMS}	B_{avg}^1
	[T]	[%]	[T]	[T]
M1	0.91	33.87	0.68	0.59
M2	0.86	34.38	0.64	0.54
M3	0.78	34.39	0.58	0.47

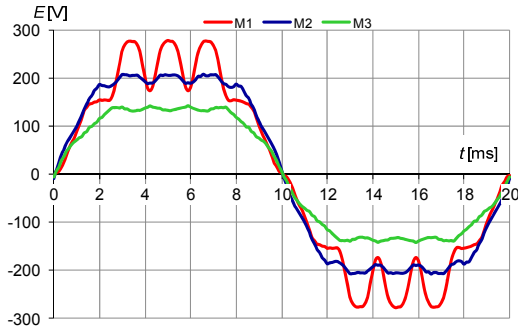


Fig. 4. Waveforms of the phase back emf induced at rated speed and no load condition (red curve M1, blue curve M2 and green curve M3)

The same as for distribution of the radial component of the magnetic flux density the Fourier analysis of determined back emf waveforms for selected structures of the rotors has been performed. The summary report has been given in Table 2.

Table 2. Summary report of the phase back emf at no load state for the selected rotors

Rotor structure	E_1	THD_{emf}	E_{RMS}	E_{avg}^1
	[V]	[%]	[V]	[V]
M1	262.19	17.24	188.14	167.39
M2	236.35	18.43	169.95	158.46
M3	159.05	17.14	114.11	106.41

The impact of the radial placement of the permanent magnet and width of the magnetic bridge on the cogging torque has also been examined. Determined characteristics of the cogging torque T_c as a function of the angular position of the rotor, for the selected rotors M1, M2 and M3 have been compared in Fig. 5. The maximal value of the cogging torque T_{cmax} reaching 1.5 Nm was captured for the motor with the rotor denoted as M1. It has been found that value of the cogging torque also decrease with the increase of the distance between magnet and the air-gap of the machine.

In the next step the impact of the magnetic barrier shape on the effective electromagnetic torque T_{av} vs. torque angle α have been examined. The model has been suited to determine torque vs. angle characteristics for given the RMS value of the supply current i_{ph} . To determine the value of the electromagnetic torque at given current i_{ph} and angle α it has been assumed that machine is supplied from 3 phase balanced system of the currents and rotor of the machine rotates with the synchronous speed. The waveform of the electromagnetic torque is determined for two periods of the supply currents for given value of the torque angle between rotor and stator filed axes. The average value of the obtained waveform T_{av} is treated as an effective electromagnetic torque and represents a single point of the characteristics shown in Fig. 6. On the basis of the obtained torque waveforms the torque pulsation factor ΔT_{el} can be determined using following formula [6]

$$(2) \quad \Delta T_{el} = \frac{T_{elmax} - T_{elmin}}{T_{av}} 100\%$$

where: T_{elmax} , T_{elmin} , T_{av} are respectively the maximum, minimum and average values of the electromagnetic torque waveform captured in one or integer number of the supply current periods.

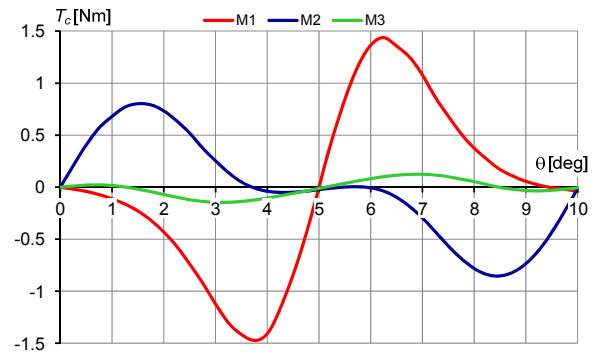
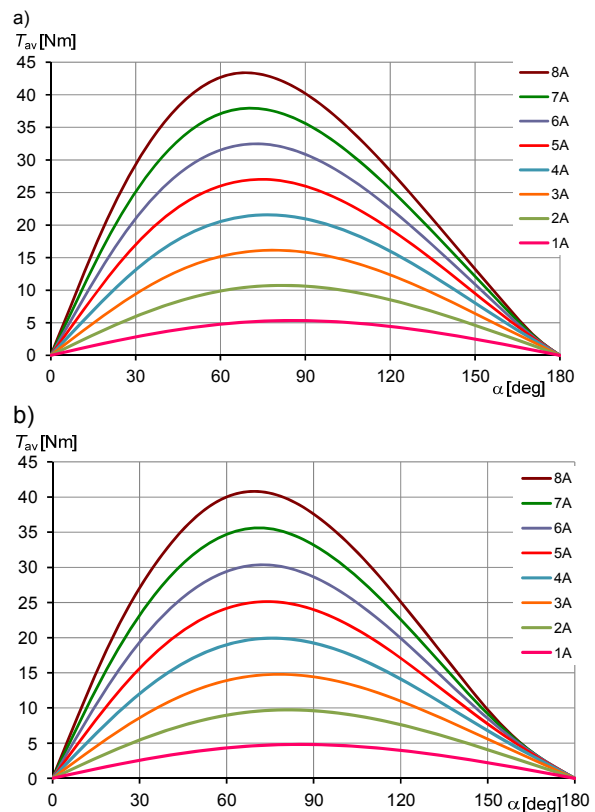


Fig. 5. Characteristics of the cogging torque vs. rotor angular position (red curve M1, blue curve M2 and green curve M3)

The values of the torque pulsation factor, average electromagnetic torque and maximum cogging torque for the studied rotor structures have been summarized in Table 3. The effective torque and torque pulsation factor have been calculated for the phase current equal to 6A and torque angle determined iteratively to achieve maximum average value of the electromagnetic torque waveform.

Table 3. Calculated average values of the electromagnetic torque T_{av} , maximal values of the cogging torque T_{cmax} and torque ripple factor ΔT_{el} ($\alpha = \alpha_{max}$, $i_{ph} = 6A$)

Rotor structure	M1	M2	M3
T_{av} [Nm]	32.45	30.34	23.78
T_{cmax} [Nm]	1.48	0.85	0.15
ΔT_{el} [%]	34.25	14.03	19.72



¹ Value determined for the pole pitch

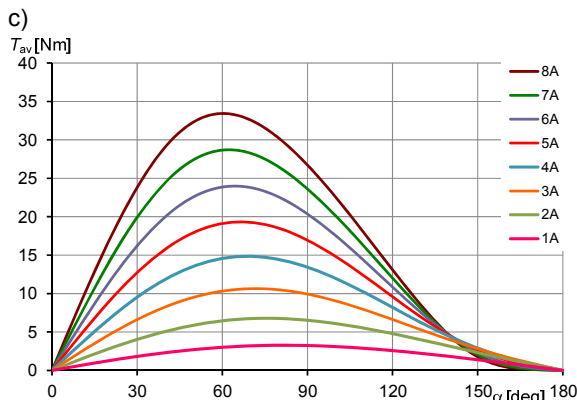


Fig. 6. The families of torque vs. angle characteristics for selected values of currents determined for rotor structures: a) M1; b) M2; c) M3

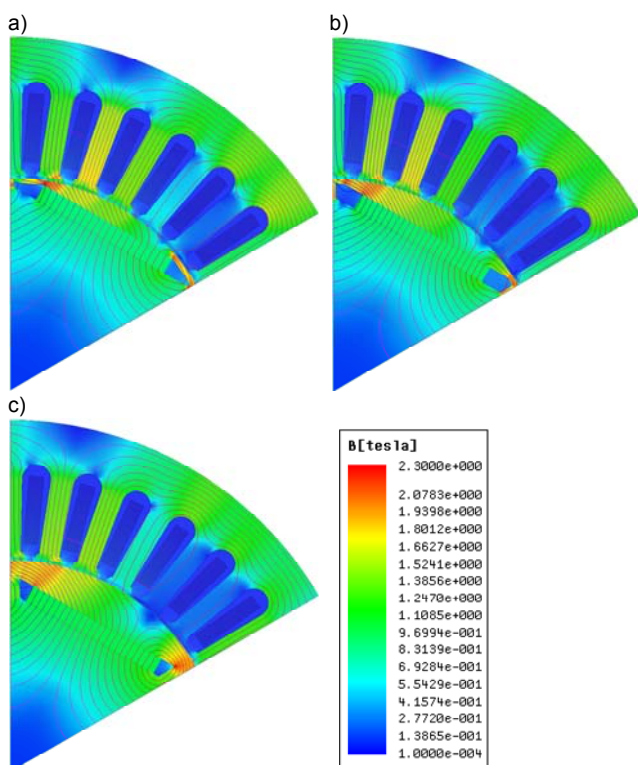


Fig.7. Magnetic field distribution for $i_{ph} = 6A$ and variants: a) M1; b) M2; c) M3

The families of the effective torque vs. torque angle characteristics for the selected values of the phase currents have been shown in the Fig. 6a), b) and c) for the motors with rotor denoted as M1, M2 and M3 respectively.

The comparison of the magnetic flux density and flux lines distributions determined for the load condition has been shown in Fig. 7. In the simulations it has been assumed that motors are supplied from the 3 phase balanced current source with phase of the RMS value equal to 6A and the torque angle is determined iteratively to achieve maximum average value of the electromagnetic torque waveform.

Conclusions

Obtained results show that the highest value of the flux leakage occurs in the structure M3, i.e. when the width of the magnetic bridges is high. Looking at the functional parameters the torque (K_t) as well as voltage (K_v) constants are the lowest. However, studying comparisons of the cogging torque, total harmonic distortion factor of the back

emf waveforms (THD_{emf}) and torque pulsations are higher for motors with the rotors M1 and M2.

On the basis of performed analyses it was found that for the design of the IPM motors with tangential magnets to reduce the flux leakage and increase motor performance it is appropriate to use as small as possible sizes of magnetic bridges. However, it should be noted that the proper value of the sizes of the magnetic bridges, besides improving the performance factors like the efficiency or the torque and voltage constants should also guarantee the low values of the cogging torque, the total harmonic distortion factor of the induced back emf and the electromagnetic torque ripple factor.

The additional limitations of the width of the magnetic bridges, which should be taken into account during the design process of the IPM machines, are the mechanical aspects concerning the mechanical stress distribution caused by centrifugal and magnetic forces.

Authors: dr hab. inż. Wiesław Lyskawinski, dr inż. Dorota Stachowiak, dr inż. Cezary Jedryczka Poznan University of Technology, Piotrowo 3a, 60-965 Poznań, Poland, E-mail: Wiesław.Lyskawinski / Dorota.Stachowiak / Cezary.Jedryczka @put.poznan.pl

REFERENCES

- [1] Alotto P., Barcaro M., Bianchi N., Guarnieri M., Optimization of Interior PM Motors With Machaon Rotor Flux Barriers, *IEEE Trans. Magn.*, 2011, Vol.47, 958-961
- [2] Barański. M., Idziak P., Łyskawiński W., Szeląg W., *Analysis of power parameters of the squirrel cage motor and LSPMS motor with U-shaped magnets*, Electrical Review, No 4/2015, pp. 135-138
- [3] Fang L., Kim S-I., Kwon S-O., Hong J-P., Novel Double-Barrier Rotor Designs in Interior-PM Motor for Reducing Torque Pulsation, *IEEE Trans. Magn.*, 2010, Vol. 46, pp. 2183-2186
- [4] Im J-B, Kim W, Kim K., Jin C-S, Choi J-H, Lee J, *Inductance calculation method of synchronous reluctance motor including iron loss and cross magnetic saturation*, IEEE Transactions on Magnetics, 2009, Vol. 45, No. 6, pp. 2803-2806
- [5] Jagiela M., Grabiec T., *Coupling electromagnetic (FE) models to multidomain simulator to analyse electrical drives and complex control systems*, Archives of Electrical Engineering, 2010, Vol. 59, No. 3-4, pp. 189-201
- [6] Jedryczka C., Łyskawiński W., Stachowiak D., *Analysis of saturation of the air gap zone in the internal permanent magnet synchronous motor (IPMSM) with "V" shape arranged magnets*, Pomiary Automatyka i Kontrola, 2013, Vol. 59, s. 1089-1092
- [7] Jedryczka C, Wojciechowski R.M, Demenko A., *Finite element analysis of the asynchronous torque in LSPMSM with non-symmetrical squirrel cage winding*, International Journal of Applied Electromagnetics and Mechanics (IJAEM), 2014, Vol.46, No.2., pp. 367-373
- [8] Kolehmainen J., Ikaheimo J., *Motors with buried magnets for medium-speed applications*, IEEE Transactions on Energy Conversion 2008, Vol. 23, pp. 86-91
- [9] May H., Palka R., Paplicki P., Szkolny S., Candlers W.-R.: *Modified concept of permanent magnet excite synchronous machines with improved high-speed features*. Archives of Electrical Engineering, 2011, Vol. 60, No. 4, pp. 531-540
- [10] Mlot A., Korkosz M., Łukaniszyn M., *Iron loss and eddy-current loss analysis in a low-power BLDC motor with magnet segmentation*. Archives of Electrical Engineering, 2012, Vol. 61, No. 1, pp. 33-46
- [11] Rahman M., Zhou P., *Determination of saturated parameters of PM motors using loading magnetic fields*, IEEE Transactions on Magnetics, 1991, Vol. 27, No. 5, pp. 3947-3950
- [12] Skarrie H., *Design of powder core inductors*. Lund University, Lund 2001
- [13] Wojciechowski R.M., Jedryczka C, Łukaszewicz P., Kapelski D., *Analysis of high speed permanent magnet motor with powder core material*, COMPEL – The International Journal for Computation and Mathematics in Electrical and Electronic Engineering, 2012, Vol. 31, No. 5, pp. 1528-1540